IEEE Access
Multidisciplinary | Rapid Review | Open Access Journal

Received May 21, 2020, accepted June 15, 2020, date of publication June 22, 2020, date of current version July 3, 2020.

Digital Object Identifier 10.1109/ACCESS.2020.3004185

Dynamic Frequency and Overload Management in Autonomous Coupled Microgrids for Self-Healing and Resiliency Improvement

S. M. FERDOUS[1], (Student Member, IEEE), G. M. SHAFIULLAH[1], (Senior Member, IEEE), FARHAD SHAHNIA[1], (Senior Member, IEEE), RAJVIKRAM MADURAI ELAVARASAN[2], AND UMASHANKAR SUBRAMANIAM[3], (Senior Member, IEEE)

[1]Discipline of Engineering and Energy, Murdoch University, Perth, WA 6150, Australia
[2]Department of Electrical and Electronics Engineering, Sri Venkateswara College of Engineering, Chennai 602117, India
[3]Renewable Energy Laboratory, Faculty of Engineering, Prince Sultan University, Riyadh 11586, Saudi Arabia

Corresponding authors: G. M. Shafiullah (gm.shafiullah@murdoch.edu.au) and S. M. Ferdous (sm.ferdous@murdoch.edu.au)

This work was supported by the Australian Government and Murdoch University through the Research Technical Program Scholarship.

ABSTRACT Autonomous microgrids (MGs) are being installed in large remote areas to supply power where access to the utility grid is unavailable or infeasible. The power generation of such standalone MGs is largely dominated by renewable based energy sources where overloading or power deficiencies can be common due to the high intermittency and uncertainty in both load and power generation. Load-shedding is the most common mechanism to alleviate these problems to prevent system instability. To minimize load-shedding, most MGs are equipped with local battery energy storage (BES) systems to provide additional support. Furthermore, in the event of severe overloading or when BES capacity is insufficient to alleviate the overload, neighboring MGs can be provisionally coupled to provide mutual support to each other which is a more effective, economic and reliable approach. Such a coupling is preferred to be via power electronic converters to enhance the autonomy of the MGs. This paper proposes a two-stage, coordinated power sharing strategy among BESs and coupled MGs for overload management in autonomous MGs, through dynamic frequency control. Both local BES and the neighboring MGs can work in conjunction or individually to supply the required overload power demand. For this, BES' state of charge should be above a minimum level and extra power generation capacity needs to be available in the neighboring MGs. A predefined framework with appropriate constraints and conditions, under which the power exchange will take place, are defined and formulated. The proposed mechanism is a decentralized approach, operating based on local frequency and state of charge measurements, and without any data communication amongst the MGs. The dynamic performance of such a network, is evaluated through extensive simulation studies in PSIM® and verifies that the proposed strategy can successfully alleviate the overloading situation in the MGs through proper frequency regulation.

INDEX TERMS Battery energy storage, dynamic frequency control, interconnection converter, coupled microgrids, overload management.

NOMENCLATURE

BES	Battery energy storage
BFC	Battery frequency controller
BSC	Battery storage converter
DER	Distributed energy resource
ICC	Interconnection converter
IFC	Interconnection frequency controller
LPF	Low pass filter
LQR	Linear quadratic regulator
MG	Microgrid
MGCC	Microgrid central controller
PCC	Point of Common Coupling
PI	Proportional-integral

The associate editor coordinating the review of this manuscript and approving it for publication was Amjad Anvari-Moghaddam.

SoC State of Charge
VSC Voltage source converter

I. INTRODUCTION

Microgrids are small-scale electrical power networks consisting of multiple distributed energy resources (DERs) and loads that can operate in a grid-connected or autonomous mode [1]. In large remote areas, where access to the utility grid is unavailable or infeasible (due to cost and economic constraint), an autonomously operating MG is the optimum and feasible electrification solution [1]–[3]. Such MGs can significantly reduce the levelized cost of energy production; thus, network operators of remote areas prefer to operate their edge-of-the-grid or regional networks in the form of autonomous MGs enabling a high penetration of renewable sources [4]–[6]. Due to high intermittency and uncertainty associated with renewable-based DERs, overloading or power deficiency as well as over-generation can be very common in autonomous MGs which will then lead to unacceptable voltage and frequency deviation from its acceptable limits and system instability [7]. To address the issues of MG overloading, numerous mechanism and operational solutions have been suggested in the literature, out of which, load-shedding is the most common, easiest and simplest approach [8], [9]. On the other hand, risk-based planning can prevent the possibility of experiencing power shortage if intermittency and unavailability of the renewable sources are considered. However, this will result in installing large-scale energy storage system and/or oversizing DERs [10], [11]. Despite its cost, it is a common and viable practice to use floating battery energy storage (BES) units to support MGs [12], [13]. Such BES units can play a vital role during peak demand, overloading or power deficiency as they can respond faster than diesel generators or micro-turbines as they are controlled through power electronics-based voltage source converters (VSCs) [14]. Nonetheless, using large BES units to address overload power demand is cost ineffective as overloading or peak power demand are either intermittent or temporary [15], causing overdesign and oversizing of the both BES unit and its converter [16].

Temporarily coupling the neighboring MGs to each other in order to exchange power in such conditions, and thus, retaining the frequency and voltage within the acceptable limits and ensuring the system stability, has been proposed in [17] as new effective approach. Forming coupled MGs also improves and enhances system reliability [18], [19]. It is expected in future that; a remote locality will consist of several neighboring MGs in a close geographical area. Under such assumptions, the overloading or power deficiency management strategy can be realized by properly coupling two or more of those MGs [20]–[23]. An extensive architectural analysis of different coupled MGs is shown in detail in [20] while [21]–[24] have discussed the concept of coupled MGs and its operation using different types of power exchange links. A transformative architecture for coupling MGs, is proposed in [25] for improving system performance during faults. Optimal control of a grid-connected MG to form coupled MGs is demonstrated in [26], [18]. Demand sharing through an interactive control of interconnected MGs is employed in [27] for wide range of system stability. The issues of excess generation management strategy can also be solved by properly coupling two or more neighboring MGs [28]–[30]. The exchange of power among the MGs in an interconnected system is discussed in [29]–[31]. Operation of DERs within an interconnected MG is studies in [33], [34], while the interaction among the DERs are investigated in [35] and their stability limits.

The main drawback of the techniques of [21]–[24], [29] is that the coupling of MGs will be established even for a minor power deficiency or overloading. Moreover, the technique of [29] is only applicable for two MGs and is not scalable. To address this problem, a new strategy is proposed in this paper which coordinates the required power sharing mechanism between a local BES unit and neighboring MG; such that light overloading can be mitigated by the BES unit while interconnection with neighboring MG is established during severe overloading. Furthermore, the proposed technique is scalable to any number of coupled MGs.

On the other hand, the physical interconnecting link of the MGs can be based on a conventional circuit breaker or an interconnecting static switch [29]. However, each MG may have a different operator, and thus, their control structure and standards can be different from each other. Therefore, a direct physical connection reduces the autonomy of the MG. Hence, for such situations, proper isolation must be provided among the MGs so that every MG can operate autonomously while exchanging power with each other. Thus, a back-to-back power electronics-based converter is a good option in such conditions [21]–[24], [31]. The proposed approach in this paper, has been further updated to consider such preferred interconnections among MGs, for which an appropriate predefined framework and protocol are essential.

This paper proposes a two-stage coordinated power sharing between BES and neighboring MGs through two different self-healing agents, functioning in a decentralized (communication free) manner. This is realized by continuously monitoring the MG frequency and its BES unit's SoC. This information is used to cooperatively activate or deactivate two developed self-healing agents, namely, battery frequency controller (BFC) for BES unit, and interconnection frequency controller (IFC) for the coupling of MGs. The proposed mechanism and control strategy are evaluated and validated through detailed computer simulation studies using PSIM®.

The key contributions of this paper to the research field can be summarized as:

- Proposing a coordinated power exchange strategy for overloading management in autonomous MGs through internal and external support (via BES and neighboring MG),
- Formulating the appropriate conditions and constraints for power exchange levels under a decentralized

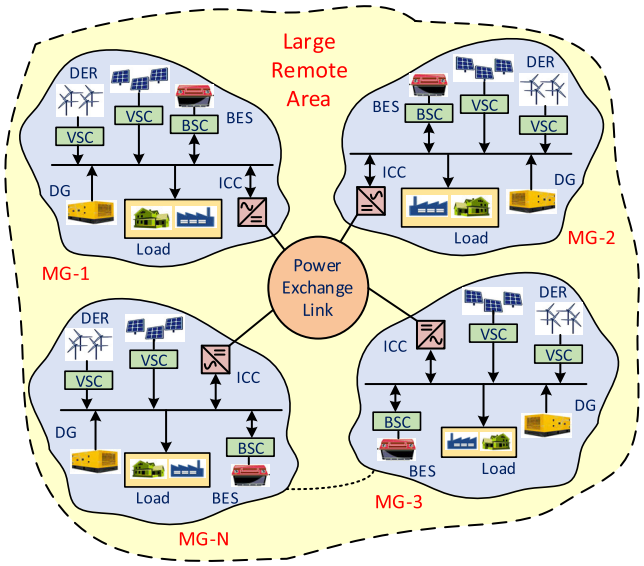

FIGURE 1. Schematic of interconnected autonomous MG networks.

approach (i.e., without any data communication amongst the MGs),

- Dynamically modifying the amount of internal and external power exchange levels based on the BES units' SoC and the MGs' loading condition

II. NETWORK UNDER CONSIDERATION

Let us consider a system of Fig. 1 where N autonomous MGs, each consisting of multiple DERs, DGs, loads, one BES and one inter-connection converter (ICC). Each MG is monitored, supervised and controlled through its MG central controller, termed as MGCC. The DERs and BES are connected to the MG through VSCs. Different VSCs are controlled in different operating modes to regulate the power and frequency of each MGs. The VSCs of DERs are assumed to be operating in the $P-f$ and $Q-V$ droop control mode, where the voltage and frequency at the output of each DER is determined from [29], [33]

$$f_{\text{MG}} = f_{\max} - m_i P_i \tag{1a}$$

$$V = V_{\text{rated}} - n_i Q_i \tag{1b}$$

where m_i and n_i are the droop coefficients of the i^{th} DER of the MG, and can be obtained from

$$m_i = \frac{f_{\max} - f_{\min}}{P_i^{\max}} \tag{2a}$$

$$n_i = \frac{V_{\max} - V_{\min}}{2Q_i^{\max}} \tag{2b}$$

where subscript $_{\max}$, $_{\min}$ and $_{\text{rated}}$ represent the maximum, minimum and rated limits for frequency and voltage of the MGs while P_i and Q_i are active and reactive powers injected by each DER to the MG. All DERs within an MG are assumed to have the same $\Delta f = f_{\max} - f_{\min}$ and $\Delta V = V_{\max} - V_{\min}$; V_{rated} is the rated voltage of the DER's PCC (i.e., one per unit) when its reactive power exchange with the PCC is zero

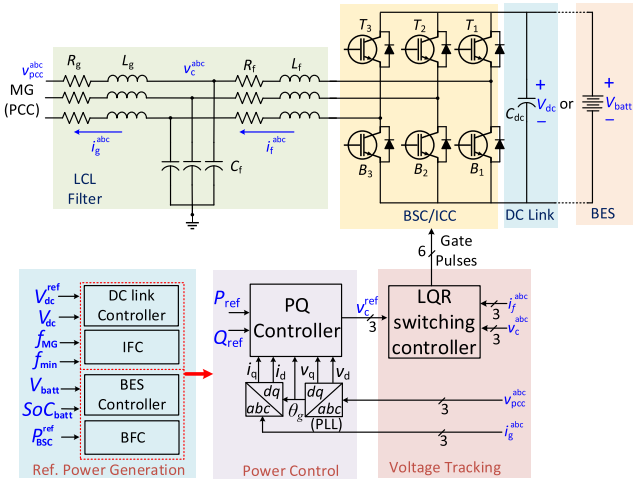

FIGURE 2. Assumed structure and closed-loop control block diagram of VSC and filter system for BSC/ICC.

(i.e., when operating at unity power factor). However, these quantities can be different in the neighboring MGs. It is assumed that, each DER is provided with its local energy storage and thus they can be represented as a dispatchable DER. The structure and operation of the DERs are discussed in [33] and is not repeated here. It should be noted that, these local storages are independent and different from the BES of each MG as the BESs are assigned to support the MGs in the event of power deficiency and dynamically regulate the frequency within the acceptable limit. The BES is connected to the MG through a separate VSC termed as battery energy storage converter (BSC) that operates in constant PQ mode. The charging or discharging mode of the BES is determined by the MGCC, based on the MG's loading condition. The detail control mechanism of BES along with its BSC, is discussed in Section IV. Finally, each MG is connected to a common dc power exchange link through its ICC to exchange power with the other MGs in the event of overloading or power deficiency. Each MG can operate independently at any predefined voltage and frequency level without affecting the operation of other neighboring MGs. The control mechanism of decentralized power exchange approach is discussed in detail in Section IV.

III. STRUCTURE AND CONTROL OF CONVERTERS

The structure of the BSC and ICC are assumed identical and their overall control block diagram are shown in Fig. 2. Both BSC and ICC are VSCs connected to their respective MG, that enable bi-directional power flow with BES and the dc power exchange link, respectively. Each converter is working in constant PQ mode and has three cascaded feedback control loops, namely, voltage tracking, power control and reference power generation loop, as can be seen from Fig. 2. The voltage tracking and power control loop are identical for both converters, whereas, the reference power generation loop, which is the most outer loop, is different and depends on the mode of operation of the MG and converter. The structure and control mechanism of the converters are discussed below:

A. CONVERTER STRUCTURE

The BSC and ICC structure is assumed to be a three-phase, three-leg VSC using IGBTs or MOSFETs, as schematically shown in Fig. 2. They are connected to the MG through an LCL filter to effectively filter out the undesired switching harmonics. The dc side of the BSC is connected to the BES while a dc capacitor is installed on the dc link side of the ICC to interconnect it to the power exchange link. It is to be noted that, any other three-phase VSC topology can also be used for BSC and ICC.

B. CONVERTER CONTROL

Both converters are operating in constant PQ mode irrespective of the loading condition of the MG. Only the respective VSC's output power reference varies depending on the MG's loading condition and the outermost control loop which is active during that time. The BSC is primarily controlled by the MGCC through the BES controller block, operating as the outermost loop. The BFC gets activated and operates in conjunction with BES controller during an overloading situation. On the other, during normal operating condition, each ICC maintains the dc link voltage of the point at which it is connected to the power exchange link. In the event of overloading and if the BES capacity is not enough to alleviate the overloading situation; IFC gets activated to import the required amount of power from the neighboring MG. The effective operation of both BSC and ICC are achieved through coordinated control among the three cascaded control loops, namely, linear quadratic regulator (LQR) based voltage tracking and switching control, power control and dc link voltage control. A brief description of these control loops is provided in Appendix-A.

IV. PROPOSED POWER EXCHANGE STRATEGY

The proposed power exchange strategy is a two-stage coordinated overload prevention mechanism for a group of coupled autonomous MGs. Let us consider each MG with the two introduced self-healing agents of BFC and IFC. All the neighboring MGs are interconnected to each other through the power exchange link and their ICCs while each MG has its own BES, connected and controlled through its BSC and MGCC respectively. To facilitate the proposed power exchange mechanism, the two self-healing agents continuously monitor the SoC of the BES and the frequency of the MG. The SoC is a measure of stored energy of BES, and hence, its capability to support the MG [36], [37]. On the other hand, the loading status of an individual MG can be determined by monitoring its frequency. As the demand of an MG increases, its frequency decreases, and vice versa. Such characteristic is due to the droop control technique employed for the DERs, as the grid-forming units of the MG and can be used as the indicator of power deficiency or overloading in an MG. Hence, there is no need for any communication link or a central controller to regulate the power flow. Furthermore, even in the presence of a central controller, the proposed power exchange mechanism can be assigned as the backup system in the event of communication failure or during any contingency. For effective power sharing among all the entities, a predefined framework needs to be introduced to identify different system parameters and their boundaries. Whether an entity (BSC/ICC) can participate in power exchange or not, must be determined by the predefined framework as their participation without proper coordination and control may lead to system instability. In general, such coordination among the entities can be done by the self-healing agents, by monitoring the MG's loading level and BES's stored energy level through frequency and SoC measurements, respectively.

During normal operation, the MGCC decides the BES's operation mode (i.e., charging/discharging) based on the MG's power generation, loading level and its frequency, f_{MG}. During overloading, if f_{MG} falls beyond the minimum value of $f_{\min}$, then first the BFC would respond to alleviate the overload situation and will work in conjunction with the BES controller. The BFC would determine the amount of excess power that needs to be provided by the BES to return the MG's frequency back to $f_{\min}$. The operation of BFC is dictated by the SoC of BES and the maximum power that can be handled by the BSC, $P_{\mathrm{BSC}}^{\max}$. In case of severe overloading, the BES may not be capable enough to alleviate the situation just by itself due to the reasons such as- the BSC reaching the maximum limit of its rated capacity and/or the SoC level not being large enough to provide the required power. Hence, the self-healing agent of IFC will then get activated to import power from the neighboring MGs. The exchange of power through interconnection can be achieved in two ways- first, a portion of the overload power demand is mitigated by the BES and the rest is provided by the neighboring MGs; second, the total overload power demand is mitigated by the power imported from the neighboring MGs assuming that they have excess power generation available. The overall block diagram of the proposed power exchange mechanism is shown in Fig. 3.

A. BES CONTROL

The control mechanism of BES during charging and discharging mode, is developed based on its SoC level, $SoC_{\mathrm{batt}}(t)$, and excess available power of the MG, $P_{\mathrm{ex}}(t)$, respectively. Both parameters are instantaneous and vary with respect to time. Different methods of measuring $SoC_{\mathrm{batt}}(t)$ are discussed in detail in [36]. On the other hand, $P_{ex}(t) = \sum P_{DER}(t) - \sum P_L(t)$ where $\sum P_{DER}(t)$ is the instantaneous total generated power of all DERs in MG and $\sum P_L(t)$ is the MG's total instantaneous demand. Since the stored energy of a BES system reduces overtime during discharging mode, it is a more practical approach to set the BES discharge power as a function of SoC instead of its ratings [15], [25], [37]. Hence, a BES system with lower SoC level can be expected to inject less power to prevent its fast discharging. Thus, the output reference power, $P_{\mathrm{batt}}^{\mathrm{dis}}$, of the BES unit during discharge mode, can vary proportionally to its SoC level in

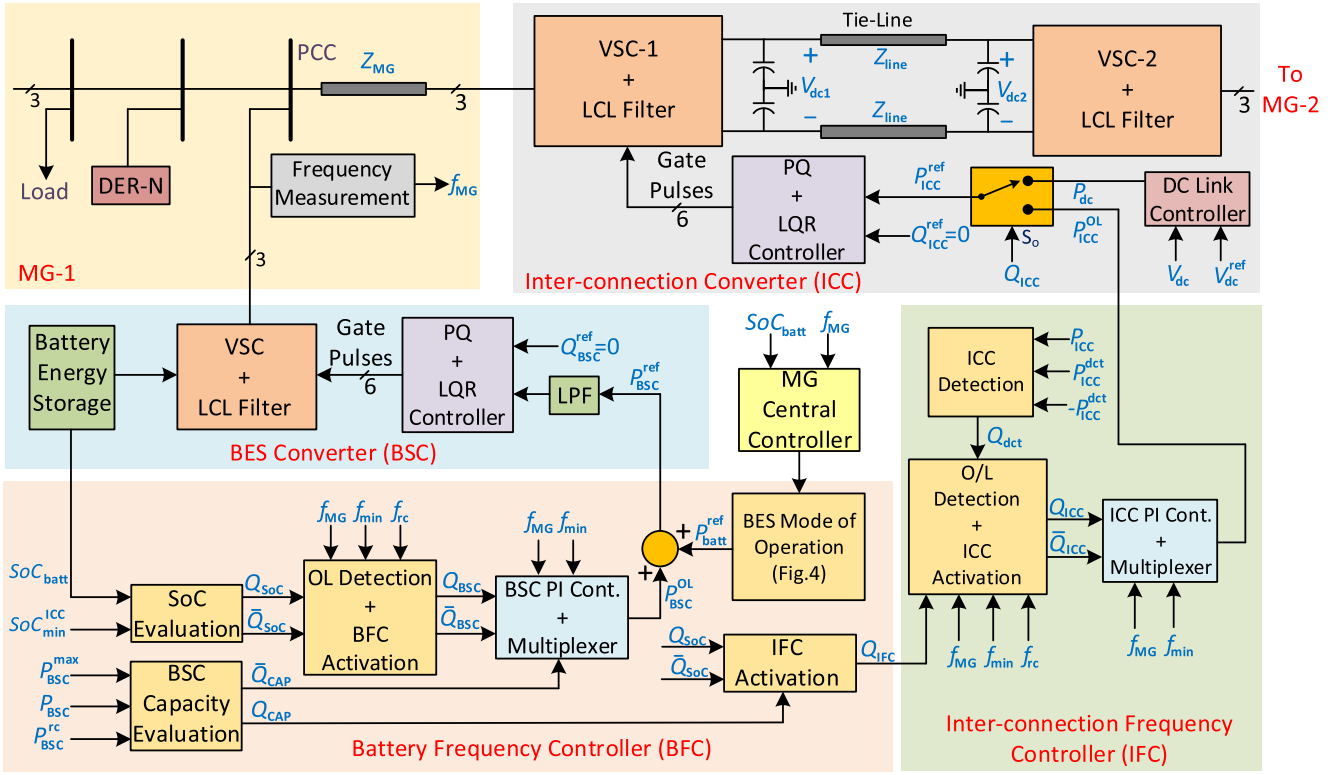

FIGURE 3. Overall block diagram of the proposed power exchange mechanism.

discrete steps (e.g., in steps of 5-10% as SoC level varies dynamically) [12], [37]. It may be noted that, the BES system will stop discharging if the SoC level drops to its minimum value of $SoC_{\min}$. The BES cannot discharge further unless it is charged up to a value of SoC_{nom}. Such a control mechanism can be implemented using a hysteresis controller.

Similarly, the charging power of the BES unit can be varied proportionally to P_{ex} in discrete steps of 5-10%. The higher is the surplus power available through excess generation of DERs in the MG, the larger is the charging power for the BES unit, and vice versa. A graphical illustration of charging and discharging power variation in discrete steps as a function of MG's surplus power and BES' SoC level respectively is shown in Fig. 4. It is to be noted that, the BES charging and discharging mode is selected based MG's nominal frequency of f_{nom}. The charging mode is enabled when $f_{\text{MG}} > f_{\text{nom}}$ as this indicates availability of surplus power generation in MG whereas the discharging mode is enabled when $f_{\text{MG}} < f_{\text{nom}}$ as this condition characterizes the loading level where the MG needs support from the BES unit. The flowchart of Fig. 5 shows the steps of operation of BES during its different operating modes while the schematic of the BES controller is shown in Fig. 6.

A distinctive feature of the proposed method is that the BES is operating in grid-following mode (constant PQ control) instead of the typical grid-forming mode (droop control) to provide the necessary support for the MG. Hence, it is controlled and monitored through the MGCC. This proposed mechanism offers better control and more flexibility in power

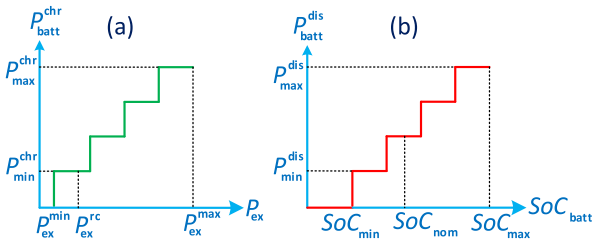

FIGURE 4. BES nominal operation scheme- (a) charging mode (b) discharging mode.

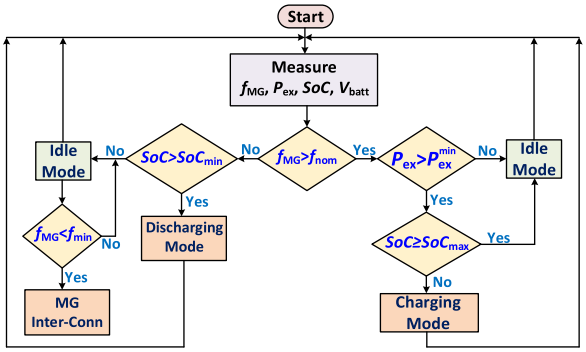

FIGURE 5. Different mode of operation of BES.

sharing via BES units. Also, the stability issues associated with droop control are eliminated; as in droop control technique, it is important to select the proper droop coefficients to ensure system stability [12], [37]. Most of the commercially available batteries are needed to be charged in constant

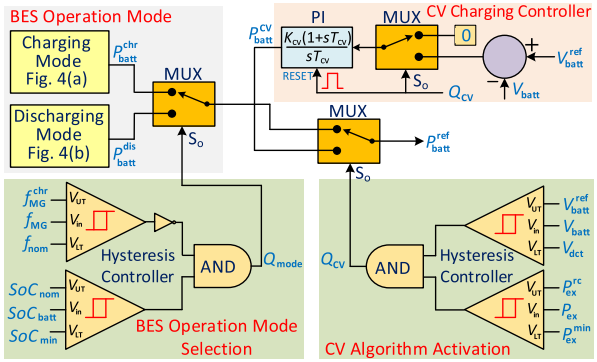

FIGURE 6. Control of BES different operation modes.

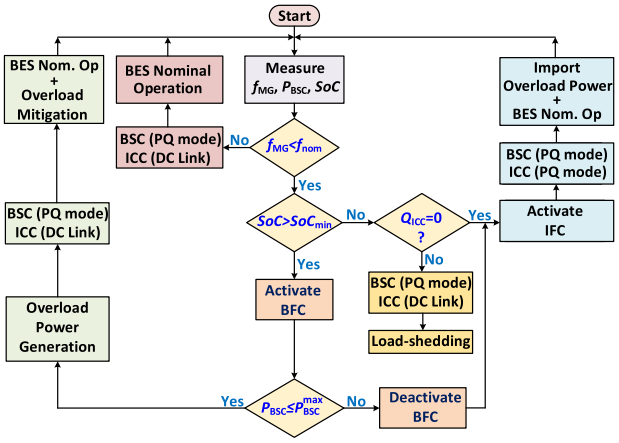

FIGURE 7. Proposed overload management scheme and its different modes of operation.

current-constant voltage mode for optimum performance and longer lifecycle, also known as healthy charging [38]. Such CC-CV charging approach is not realizable in droop control technique. But with the proposed BES control mechanism, constant-voltage healthy charging mode can be easily implemented as shown in Fig. 6.

B. CONTROL OF BFC AND BSC

The BFC is the outermost control loop that gets activated and operates in conjunction with the BES controller and regulates the output power of BSC during overload situation. To better understand the operation of BFC and BSC, let us consider the flowchart of Fig. 7. During nominal operating condition of the MG, the BSC will receive the power reference from BES controller and the charging/discharging mode will be decided based on the developed logic. The BFC will only get activated during discharge mode when there is no surplus power generation available in MG. Thus, the activation and operation BFC is governed by f_{MG}, SoC_{batt} and $P_{\mathrm{BSC}}^{\mathrm{max}}$. The functional block diagram of BFC is shown in Fig. 8. In the event of overloading, if f_{MG} drops below f_{min}, the BFC will get activated through the control signal of Q_{BSC} after a certain time delay of t_{act}^{B}, if the BES SoC level is greater than the minimum value of $SOC_{\mathrm{min}}^{\mathrm{ICC}}$. If not, then BFC will not get activated as the SoC level of BES unit is not enough to

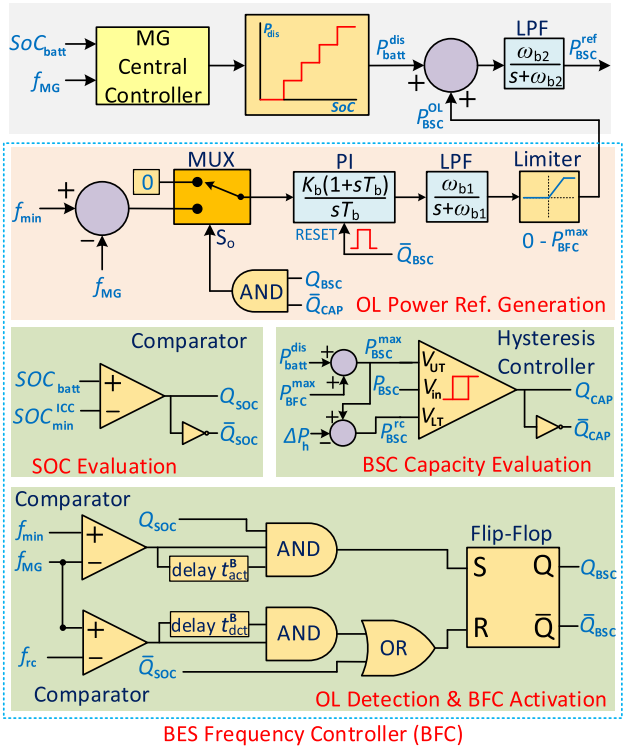

FIGURE 8. Control mechanism of BSC for overload management.

alleviate the overload, and hence, power needs to be imported from neighboring MGs via the ICC. Similarly, when the overloading period of the MG is over, the BFC will get deactivated and the proportional-integral (PI) controller is reset after a certain delay of t_{dct}^{B}. The input signal fed to the PI controller is controlled through a multiplexer to ensure proper operation and to avoid drift in PI controller. A low pass filter (LPF) is added to introduce a certain delay to match the battery response time. It is to be noted that, the delays are essential to allow a reasonable time for the system transients to settle down. Without a proper delay, it is highly possible that the self-healing agents are activated even during transients which will result in redundant and unnecessary of power sharing.

Another mode of operation of BFC is possible when, the SoC level can only alleviate a portion of the total overload. Hence, the total overload power demand needs to be shared by the BES systems of the overloaded MG and its neighboring MGs. This is realized by the BSC capacity evaluation block of the BFC and dynamically varying the parameter, $P_{\mathrm{BSC}}^{\mathrm{max}}$ as a function of the SoC. The arrangement is shown in Fig. 8. $P_{\mathrm{BFC}}^{\mathrm{max}}$ is the maximum reference power generated by the PI controller of BFC and P_{BSC} is the measured output power of BSC. When P_{BSC} reaches its maximum limit of $P_{\mathrm{BSC}}^{\mathrm{max}}$, the input of PI controller should be set to zero. The reset command of PI controller should not be activated at this instant as the controller must retain the value at its output. The output power reference produced by the PI controller is the portion of overload power demand that can be supplied by the BES unit as per its SoC level. The rest of the overload power demand must be supplied by the neighboring MGs.

Hence, an activation command for the ICC must be produced to initiate the power sharing through the power exchange link.

C. CONTROL OF IFC AND ICC

The second self-healing agent of the MG is IFC which is responsible for importing power from the neighboring MGs through the power exchange link. The IFC is one of the outermost control loops for ICC. The activation of IFC depends on two specific conditions. First, when the SoC level of BES is less than $SoC_{\min}^{\text{ICC}}$, i.e., the SoC level is not large enough to supply the required overload power demand. In this case, the entire overload power demand is supplied by the ICC from the neighboring MGs. Second, when the BSC reaches its maximum power limit while supplying overload demand as explained in previous section. Hence, the rest of the overload power demand must be imported from the neighboring MG through the ICC. These two conditions are used to derive the activation logic, Q_{IFC}, to activate the IFC which enables the ICC to import required power for the overloaded MG. The functional block diagram of the IFC is shown in Fig. 9. The structure and function of the controller is similar to BFC. During nominal operation of the MG or while a healthy MG supporting a neighboring overloaded MG, the ICC should operate in the dc link voltage control mode while the IFC must remain deactivated. However, if the healthy MG that was supporting an overloaded MG, becomes overloaded too, the local BES system of the healthy MG and its BFC should get activated to alleviate the overload situation as long as the overload power is less than $P_{\text{BSC}}^{\max}$ of that particular MG. If the overload power exceeds $P_{\text{BSC}}^{\max}$, then there is no alternative other than to initiate load shedding. This is achieved by the activation logic of Q_{ICC}, as can be seen from Fig. 9. A logic low value of Q_{ICC} indicates that, the MG is already supporting another neighboring overloaded MG and the ICC must operate in the dc link voltage control mode, while IFC should remain deactivated. The steps of operation of the control approach in such case can be interpreted from the flowchart of Fig. 7. The sequence of control logic is necessary to implement the developed decentralized control approach. Otherwise, the interconnection among the MGs will lead to instability throughout the entire system.

V. PERFORMANCE EVALUATION

To evaluate the dynamic performance of the proposed control, let us consider the system of Fig. 1 with two (for study cases A-E) and three MGs (for study case F) are connected through a dc power exchange link, respectively. The performance of such a system has been evaluated through six study cases, as illustrated schematically in Fig. 10 and discussed seperately in this section. In these studies, the maximum capacity of each MG is 70kW and the minimum acceptale frequency limit is 49.8Hz while The nominal frequency is 50Hz. The base power is assumed as 100 kVA while the base dc voltage in the power exchange link is assumed as 1kV.

In these study cases, to replicate non-ideal scenarios, all the power electronic converters are represented by their

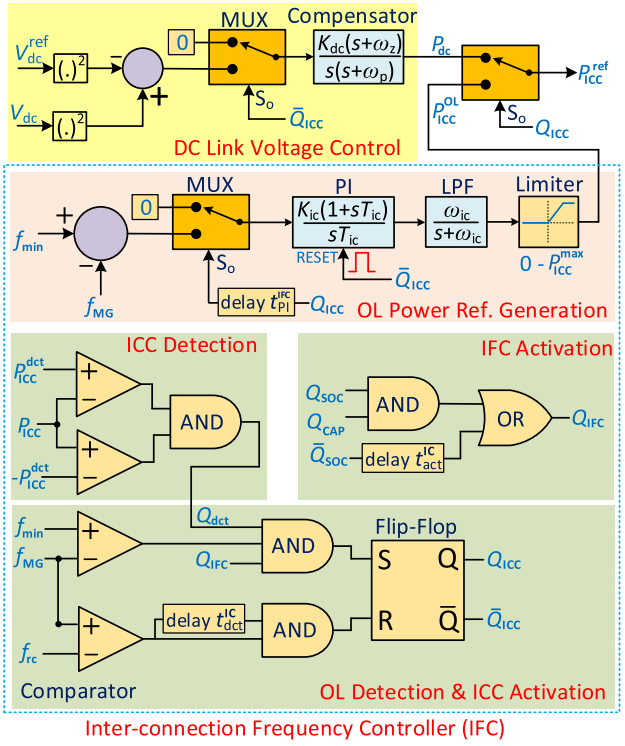

FIGURE 9. Control mechanism of ICC for overload management.

detailed switching model and the conventional close loop control systems are carefully designed with necessary gain and phase margins, so that rated power exchange can take place within the network and their stability limits. Each assumed MG also consists of two or more power electronic converter based DERs, operating under droop control, and one power electronic converter interfaced BES. Furthermore, different operating and loading conditions of the MGs and their BES are considered such as – independent/joint operation of the controllers, transition in controller actions and light/moderate/heavy overloading. All the control actions are carried out using local measurements only and without any data communication among the controllers and converters.

A. LIGHT OVERLOADING

To verify the ability of each MG operating independently and addressing the overloading problem, let us consider the network of Fig. 10a and assume that both MGs are initially operating at the steady-state condition and under the droop control. In this particular study case, both MGs will be lightly overloaded and the situation can be alleviated by their respective BES units. Hence, no external power support is required. The applied events in both MGs at different time instants are as follows while the simulation results of the MGs are shown in Fig. 11.

The BES unit of MG-1 and 2 are initially in discharging mode and respectively providing a power of 0.1 and 0.075 pu. At $t = 0.7$ s, MG-1 becomes overloaded by 15% (see Fig. 11a); hence, its frequency decreases to 49.7 Hz (see Fig. 11e). As the frequency has fallen beyond the acceptable

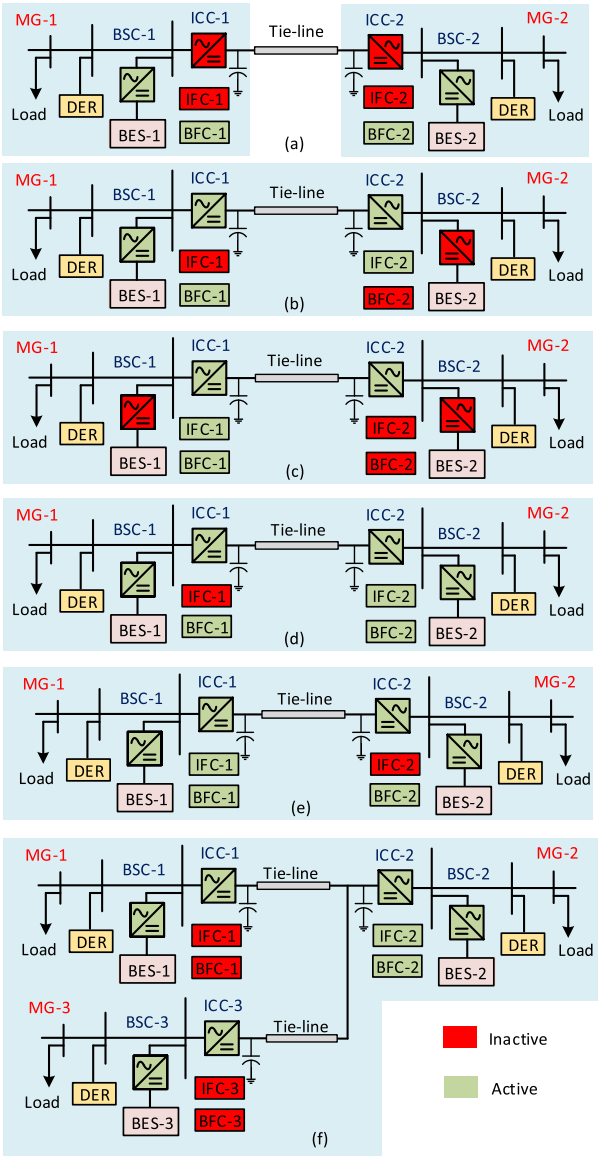

FIGURE 10. Status of self-healing agents and converters in 6 different case studies.

limit of 49.8 Hz, MG-1's BFC gets activated after a fixed delay of 0.5 s. The controller determines the amount of overload, $P^{\mathrm{OL}}_{\mathrm{BSC}-1}$, to bring the frequency back to its acceptable limit. The BES unit adjusts it reference power, $P^{\mathrm{ref}}_{\mathrm{BSC}-1}$, and starts to inject the required power to alleviate the overload situation. At $t = 2.5$ s, the BES power level has decreased from 0.1 to 0.075 pu, based on its SoC level, as decided by the MGCC. Thus the BFC again adjusts the power level through to maintain the frequency at 49.8 Hz. At $t = 4$ s, the overloading of MG-1 is removed and its goes back to normal operating condition. The BFC sets the reference overload power to zero and gets deactivated after a delay of 0.4 s. MG-1 continues to receive 0.075 pu of power from BES as decided by MGCC.

Now, let us consider the scenarios applied in case of MG-2. MG-2 was initially at the steady state condition while

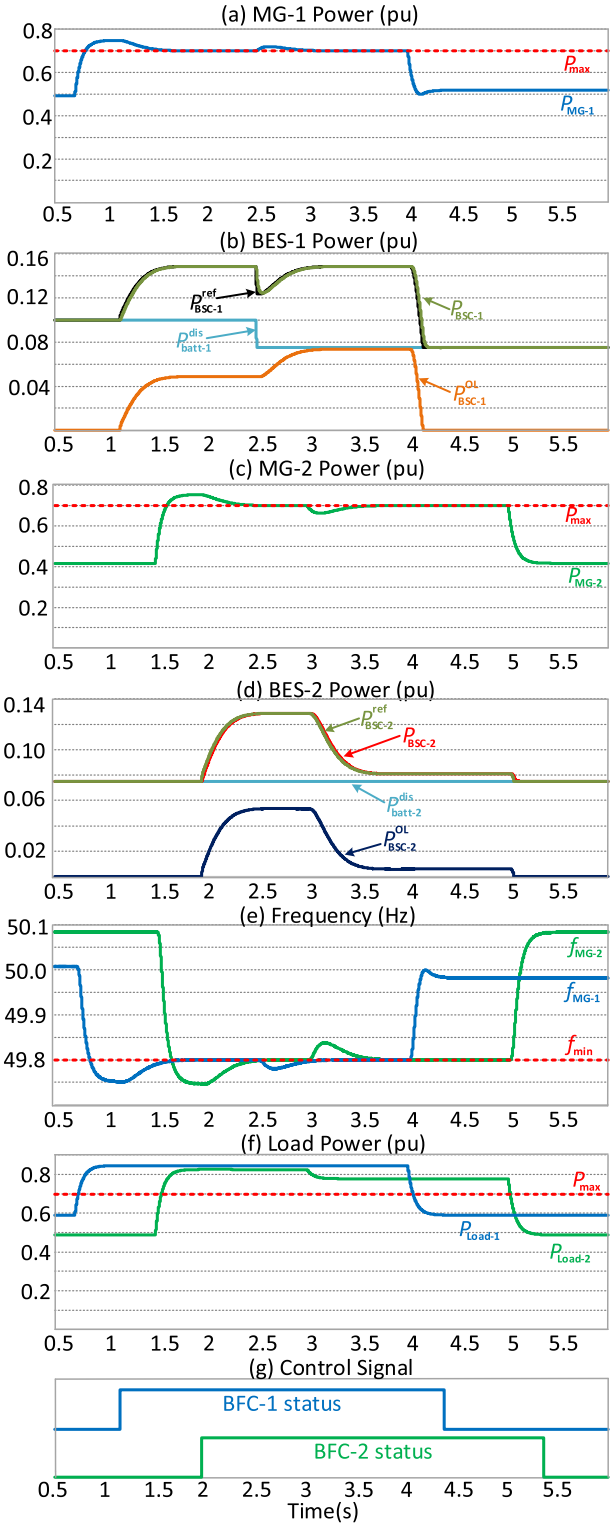

FIGURE 11. Simulation results for light overloading.

MG-1 was undergoing the overloading scenarios. As the ICC and the power exchange link provide complete isolation among the MGs, any changes in MG-1 does not affect the operation of MG-2, and thus ensures a complete autonomy in the operation of the MGs. At $t = 1.5$ s, 13% overload is applied in MG-2, and thus frequency goes below 49.8 Hz

(See Fig. 11c and 11e). The BFC of MG-2 gets activated after 0.5 s and starts to inject additional power of 0.055 pu to the MG-2 to retain the frequency back to 49.8 Hz. At $t = 3$ s, the overload is reduced by 8%, and hence the new overload level is 5%. Therefore, the BFC reduces the reference power to the new value of 0.005 pu. At $t = 5$ s, the overload is completely removed and the BFC gets deactivated after 0.4 s as the MG returns back to the normal operation.

B. MODERATE OVERLOADING

Let us assume, a scenario in which an MG is moderately overloaded but the BES unit does not have enough energy storage to alleviate the overload. At that instant, if the neighboring MG has excess power available, it can supply the required power to the overloaded MG through the power exchange link. The schematic of the conidered network is shown in Fig. 10b while the simulation results are provided in Fig. 12. Let us assume a scenario in which MG-2 is overloaded by 20% at $t = 0.3$ s, and hence its frequency drops below 49.8 Hz. During this time, the BES of MG-2 is not in operation due to its low stored energy level, i.e., the SoC of BES unit is below $SOC_{\min}^{\text{ICC}}$. As a result, the BFC remains inactive and the IFC gets activated by sensing the frequency deviation and low level of SoC. First, the IFC will change the mode of operation of ICC from dc link voltage control to constant PQ control mode. After a preset delay of 0.4 s, the IFC calculates the amount of overload power needs to be imported from MG-1 to retain the frequency back to 49.8 Hz through the ICC of MG-2. It may be noted that ICC of MG-1 will continue to operate in maintaining the dc link voltage of the power exchange link and operates in its nominal condition. A power of 0.2 pu is required to alleviate the overload situation of MG-2 as can be seen from Fig. 12c, denoted as P_{g2}. The power supplied by MG-1 is slightly higher over 0.2 pu because of the losses in the converter and tie-line as denoted by P_{g1}. At $t = 1.3$ s, an additional 15% load is added to MG-1. Due to addition of this load, while it was supporting MG-2 to alleviate its overloading, MG-1 also becomes overloaded by 5%. The SoC level of BES in MG-1 is over nominal value and was delivering a power of 0.1pu while it was overloaded. Hence, additional power needs to be supplied by the BES and thus the BFC of MG-1 is activated. It determines the required overload power to be supplied is 0.05 pu and the total output power of BSC of MG-1 is 0.15 pu, as can be seen from Fig. 12d. This scenario continues until $t = 3.2$ s at which the overloading of MG-2 is removed and MG-2's frequency increases above the minimum limit. Therefore, MG-2 goes back to the normal operating condition. As MG-1 does not need to support MG-2 anymore, the frequency of MG-1 also increases above the minimum limit of 49.8 Hz at the same time and MG-1 goes back to its nominal operating condition as soon as MG-2's overload is removed. MG-1 continues to operate nominally with additional 15% added load until $t = 4.2$ s, when the additional load is also removed from MG-1. The respective control signals for activating the self-healing agents are shown in Fig. 12f. It is to be noted that the IFC is

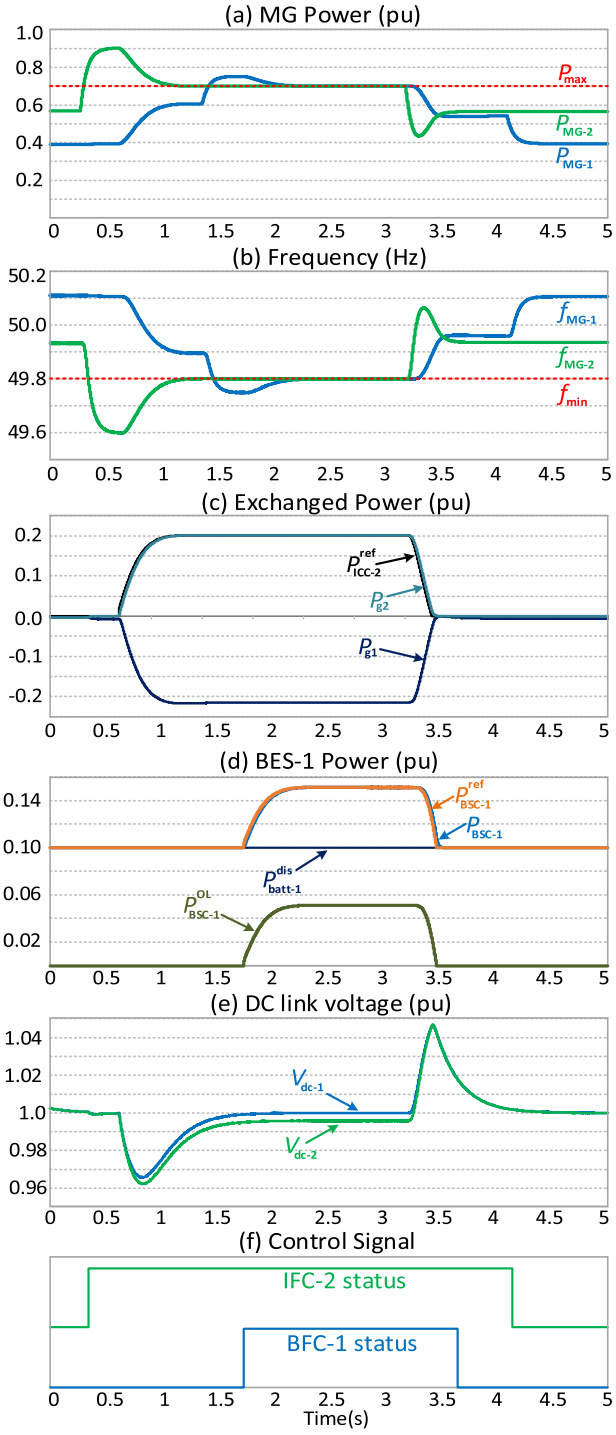

FIGURE 12. Simulation results for moderate overloading.

activated for MG-2 as it needed support through the power exchange link while BFC was activated for MG-1 as it is supported by its local BES unit. It may also be noted here that both of the IFCs must not get activated at the same time in the event overloading as there will be no convereter to regulate the voltage of the power exchange link. This is realized by the ICC detection loop (which is basically a window detector circuit) as shown in Fig. 9. The time delay in deactivation

of IFC is greater than BFC as IFC must wait for a longer period to allow the dc link voltage to settle down and reach the steady-state. When the IFC is deactivated, the control of corresponding ICC shifts from constant PQ control mode to dc link voltage control mode.

C. CONTROLLER TRANSITION

Let us consider the network of Fig. 10c and assume a scenario in which an MG is lightly overloaded and the situation can be alleviated easily just by the BES unit itself. But if the overloading continues for a long duration of time, the BES's stored energy will be depleting rapidly. As a result, the SoC level is also decreasing in proportion to its stored energy. At some point the BES will stop supporting the MG due to the lack of adequate stored energy. Therefore a transition in the control action needs to take place, i.e., the IFC should take over in the place of the BFC to alleviate the overload. This transition in control should be done smoothly and without causing any stability issues. The simulation results of this case are provided in Fig. 13. Let us assume MG-1 is operating nominally with the BES supplying a power of 0.025 pu at an SoC level of 65%. At $t = 0.2$ s, the MG is overloaded by 6%. Thus, the BFC gets actiavated and starts to supply an additional power of 0.06 pu to alleviate the overloading. Hence, the total power provided by the BES unit to the MG is 0.085 pu as can be seen in Fig. 13d. At $t = 2.35$ s, the SoC of BES in MG-1 goes below the minimum limit of $SoC^{\text{ICC}}_{\text{min}}$, which is assumed to be 55% in this study and hence the BFC gets deactivated as per the developed control logic. At this instant, the BES is providing only a power of 0.025pu, instead of required power of 0.085 pu. Hence, MG-1 becomes overloaded again and the frequency falls below 49.8 Hz. It is then sensed by the IFC and therefore, gets activated at $t = 2.5$ s. The subsequent steps of operation of IFC are exactly the same as it was in the study case-B above. IFC enables the ICC to import a power of 0.06 pu from MG-2 to alleviate the overload. This is continued until $t = 3.8$ s at which the BES of MG-1 completely stops supplying power to MG-1 as deciced by the MGCC based on its SoC level. Therefore, the IFC adjusts the required power demand to retain the frequency back to 49.8 Hz once again. The overload of MG-1 is removed at $t = 5.2$ s and it goes back to its nominal operation again. The IFC waits for a certain time for the dc link voltage to settle and then switches back to the dc link voltage control mode.

D. HEAVY OVERLOADING-1

To alleviate a heavy overloading situation, the total power may be shared between the local BES and the neighboring MG. In the event of any overloading, it is expected that the MG should first try to alleviate the problem using local BES. If the stored energy of BES or the capacity of the BSC are not enough to address the overload problem, the MG should start importing power through ICC. Both BSC and ICC should operate simultaneously to supply the overload power demand. Now, let us consider the network of Fig. 10d. Let us assume a

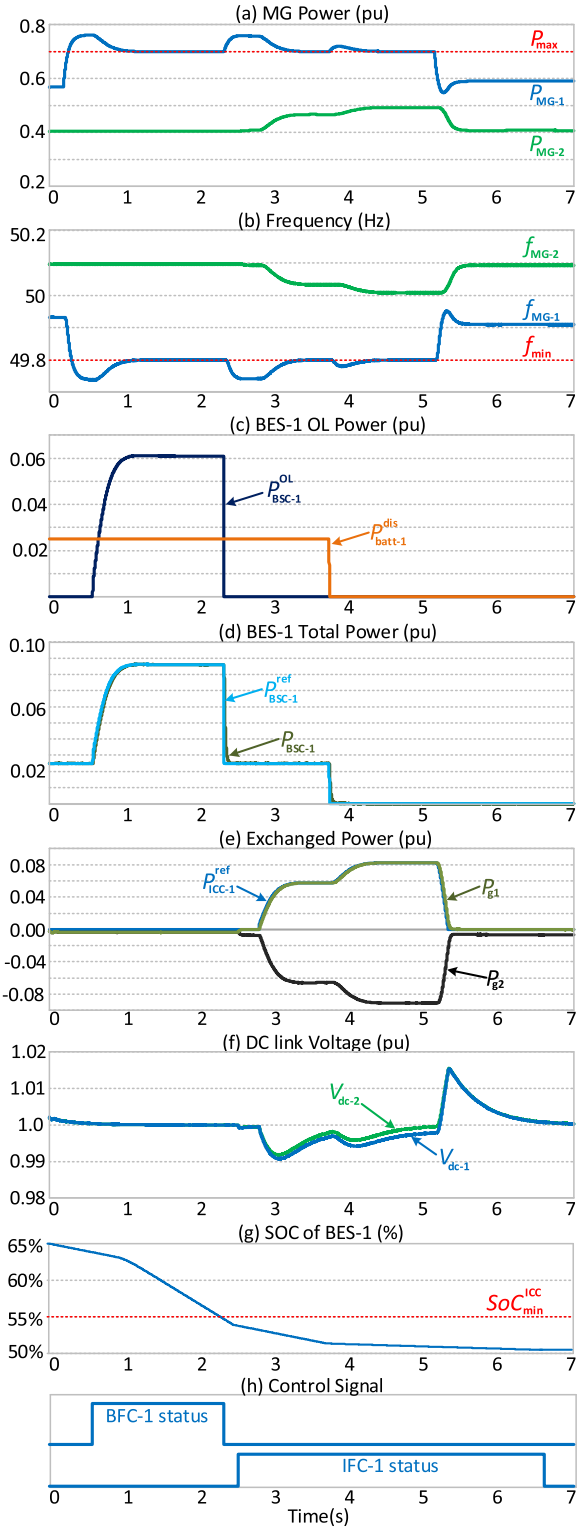

FIGURE 13. Simulation results for controller transition.

scenario where both the MGs are operating in nominal condition as can be seen in Fig. 14. The SoC level of both BESs are at maximum level. Hence both of them are supplying rated discharge power of 0.1pu to their respective MGs. At $t = 0.2$ s, 18% overload has occured in MG-2, and as a result, the

frequency drops drastically below 49.8 Hz. This situation is sensed by BFC and it gets activated at $t = 0.5$ s. At $t = 0.7$ s, the BFC starts to generate the reference power to alleviate the overload situation as can be seen from Fig. 14c. Due to heavy overloading, the required power reference produced by the PI controller exceeds the maximum rated capacity of BSC, $P_{\text{BSC}}^{\text{max}}$, which is assumed as 0.2 pu in this study. Hence, the PI controller should freeze (not reset) by setting its input to zero using the multiplexer circuit, as shown in Fig. 8. Thus, the output of the PI controller will retain the evaluated value which is the maximum power that can be delivered by the BES unit at that SoC level. This is realized by comparing the instantaneous output power of BSC, P_{BSC}, with $P_{\text{BSC}}^{\text{max}}$. The parameter of $P_{\text{BSC}}^{\text{max}}$ can be dynamically varied and evaluated based on SoC level as discussed in section IV.B and illustrated in Fig. 8. In this particular study case, $P_{\text{BSC}}^{\text{max}}$ is set based on the BSC's maximum capacity, as BES's SoC level is at its maximum level. In any other scenario, $P_{\text{BSC}}^{\text{max}}$ can be evaluated dynamically based on the BES' SoC level. This means that even though the BSC is capable to handle the required overload power, the SoC level of the BES is insufficient to produce it. Hence, $P_{\text{BSC}}^{\text{max}}$ needs to be updated dynamically based on its SoC level and such freezing mechanism of PI controller is needed for this purpose. While both BSC and BES reach their maximum power limit of 0.2 pu, the overloading of the MG is not alleviated, and hence, the frequency still stays below 49.8Hz, as can be seen from Fig. 14b and 14c. This situation makes the IFC to get activated at $t = 1.1$ s. The ICC of MG-2 changes its operation from the dc link voltage control mode to constant PQ mode and starts importing power from MG-1 at $t = 1.5$ s. Thus, the overload of the MG-2 is alleviated with both self-healing agents working simultaneously during which the BSC provides a power of 0.1 pu while the ICC supplies a power of 0.12 pu, as can be seen from Fig. 14d. Due to the rapid discharge rate of BES-2 (as it is operating at its maximum capacity due to overload), at $t = 3$ s, the MGCC reduces the power from 0.1 to 0.05 pu. Therefore, the IFC increases the ICC's power reference to maintain the frequency at 49.8 Hz. At $t = 4.5$ s, MG-1 becomes overloaded by 6%. The BFC of MG-1 gets activated and alleviates the overload situation. At $t = 7.5$ s, the overloading of MG-2 is removed, and as a result, both MGs are back to normal operation. It should be noted that, all the four converters of both MGs (i.e., 2 BSCs and 2 ICCs) were active and working in conjunction to alleviate the overload situation. The BFCs of both MGs were active whereas the IFC of only MG-2 was active (as both IFCs are not allowed to get activated simultaneously). This is realized by the activated control signals, as shown in Fig. 14h.

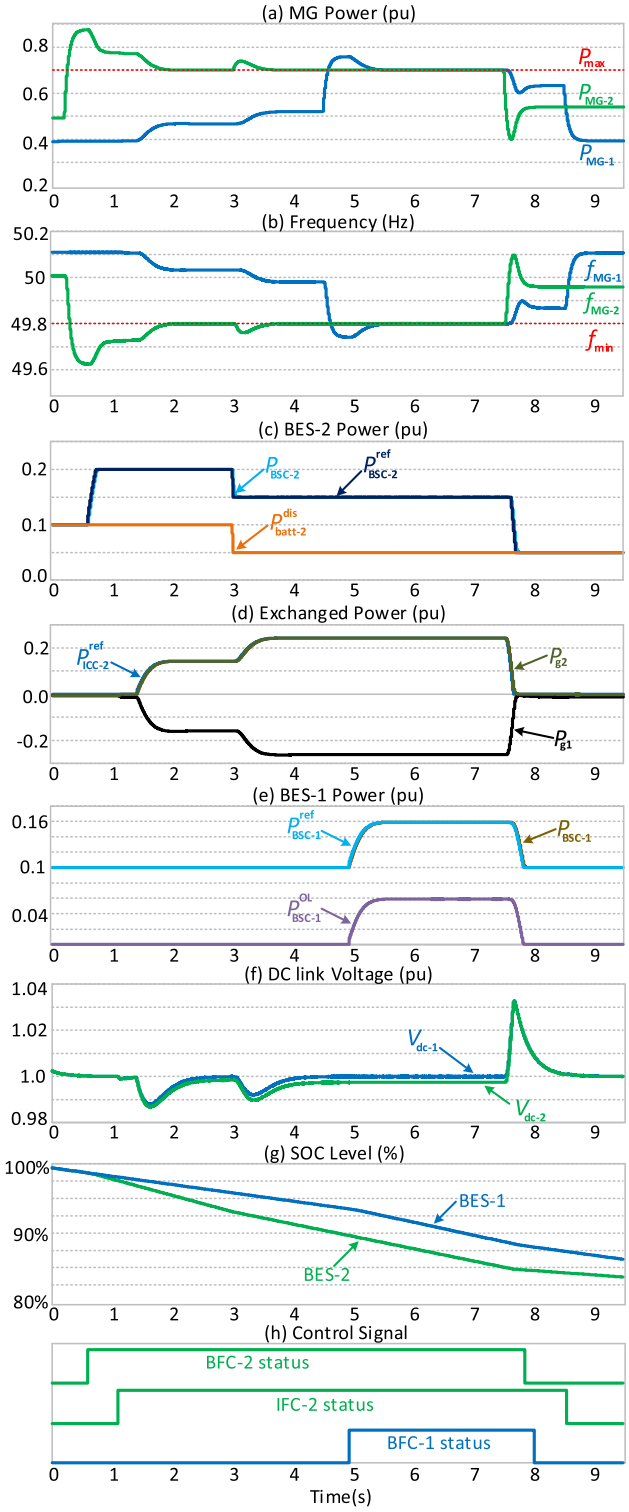

FIGURE 14. Simulation results for heavy overloading-1 example.

E. HEAVY OVERLOADING-2

To investigate the efficacy and capability of alleviating overloading situation in a decentralized manner, another heavy overloading situation is considered. This study verifies that a lightly or moderately overloaded MG which is being supported by its BES can support its heavily overloaded neighboring MG through interconnection. The proposed decentralized topology will enable the MGs to exchange power among themselves during overload situation as long as at least one IFC is inactive. In otherwords, as long as an MG exists that is capable of regulating the voltage of the power

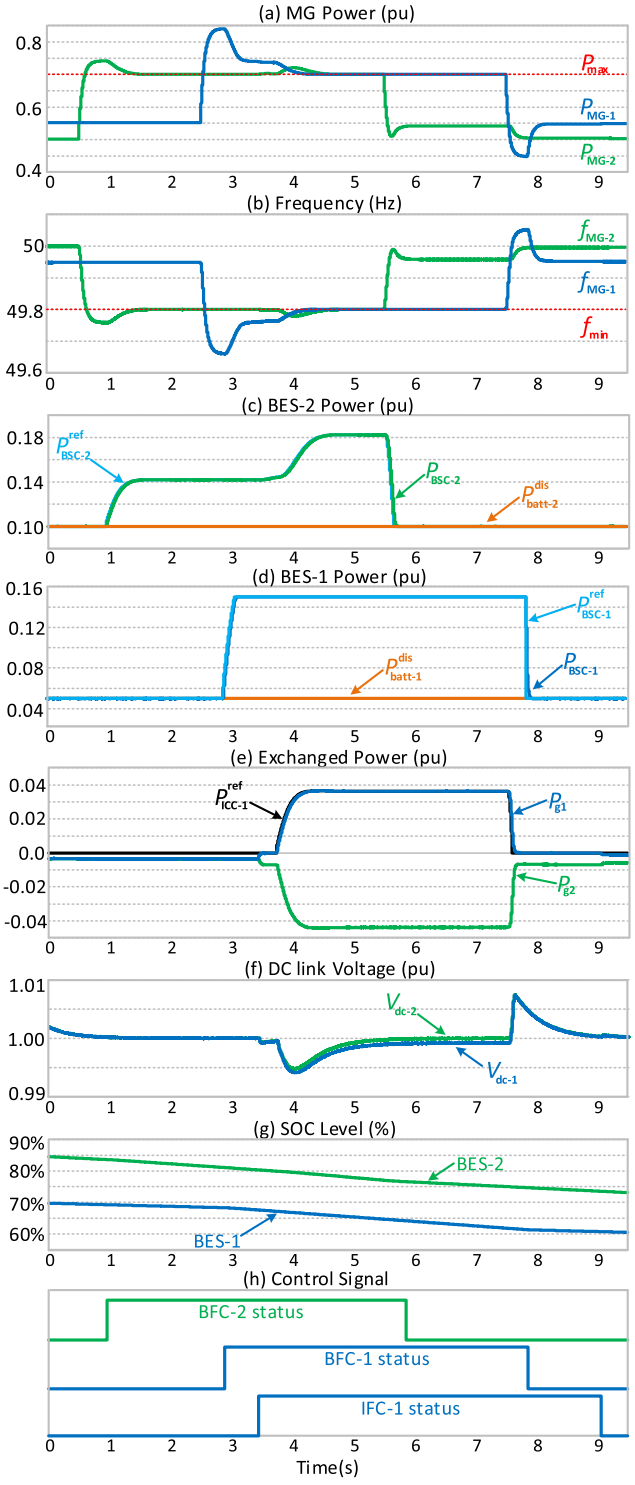

FIGURE 15. Simulation results for heavy overloading-2 example.

exchange link, the exchange of power among them can take place, even though that particular MG may be overloaded and being supported by its BES unit. Consider the network of Fig. 10e for this study while Fig. 15 illustrates the simulation results. Let us assume that at $t = 0.5$ s, MG-2 is overloaded by 5%. As a result the frequency has dropped below 49.8 Hz. BES-2 was supplying a power of 0.1pu as decided by the MGCC, at the time of overloading. The drop in frequency level activates the BFC and it adjusts the active power reference for BSC to supply the required overload power to MG-2. Thus, the frequency returns back to 49.8 Hz. The situation continues until $t = 2.5$ s at whichMG-1 becomes overloaded by 14%. At the time of overloading, BES-1 was delivering a power of 0.05 pu to the MG. This activates the BFC's associated controller. The SoC of BES-1 is less than 70% at this time as can be seen from Fig. 15g, which sets the maximum power that be supplied by BSC, $P_{\text{BSC}}^{\max}$, as 0.15 pu. In this case, the value of $P_{\text{BSC}}^{\max}$ is determined based on the BES' SoC value unlike the previous case, where it was chosen based on converter's maximum rating. Due to heavy overloading, the output of the PI controller of the BFC will reach its maximum limit of 0.15 pu within a short period of time and freezes, as can be seen from Fig. 15d. As the overloading problem is not alleviated, the IFC of MG-1 will get activated at $t = 3.4$ s. Hence, the mode of operation of the ICC of MG-1 changes from the dc link voltage control to constant PQ mode. This is a scenario where both MGs are overloaded (MG-2 is lightly and MG-1 is heavily). As the ICC of MG-1 is changed to constant PQ mode, the ICC of MG-2 must remain in the dc-link voltage control mode to regulate the voltage of the power exchange link. It is to be noted that, for a network where more than two MGs are interconnected to share power, at least one MG is needed which is not heavily overloaded and can assign its ICC to regulate the dc-link voltage of the power exchange link. Once, the IFC of MG-1 is activated, it will produce the desired reference to start importing power from MG-2, as can be seen from Fig. 15e. As such, the frequency of MG-1 retains back to 49.8 Hz and the overloading is alleviated. At $t = 5.5$ s, the overloading in MG-2 is removed and it goes back to its normal operation mode. However, MG-2 keeps on supporting MG-1, as long as it remains overloaded. At $t = 7.5$ s, the overloading in MG-1 is removed and it also moves back to its normal operation. The corresponding activation control signals for BFCs and IFC of both MGs are shown in Fig. 15h.

F. MULTIPLE MGs

This study case demonstrates the power sharing amongst multiple MGs to alleviate the overloading situation. Let us consider the network of Fig. 10f and assume a scenario in which three MGs are coupled through the power exchange link. The results of this study are provided in Fig. 16. Let us assume that all the three MGs are operating in their nominal condition. BES-1, 2 and 3 are supplying respectively a power of 0.1, 0.05 and 0.1 pu to their respective MGs, as can be seen from Fig. 16c. At $t = 0.3$ s, MG-2 is overloaded by 22%, and as a result, the frequency drops below 49.8 Hz. This activates the controller of BFC-2 at $t = 0.6$ s. Based on the SoC level of BES-2, the maximum power that be supplied, $P_{\text{BSC}}^{\max}$, is evaluated as 0.15 pu. As soon as the output power of BSC-2 reaches 0.15 pu, the controller of BFC-2 freezes, as can be seen from Fig. 16c. As the frequency of MG-2 is

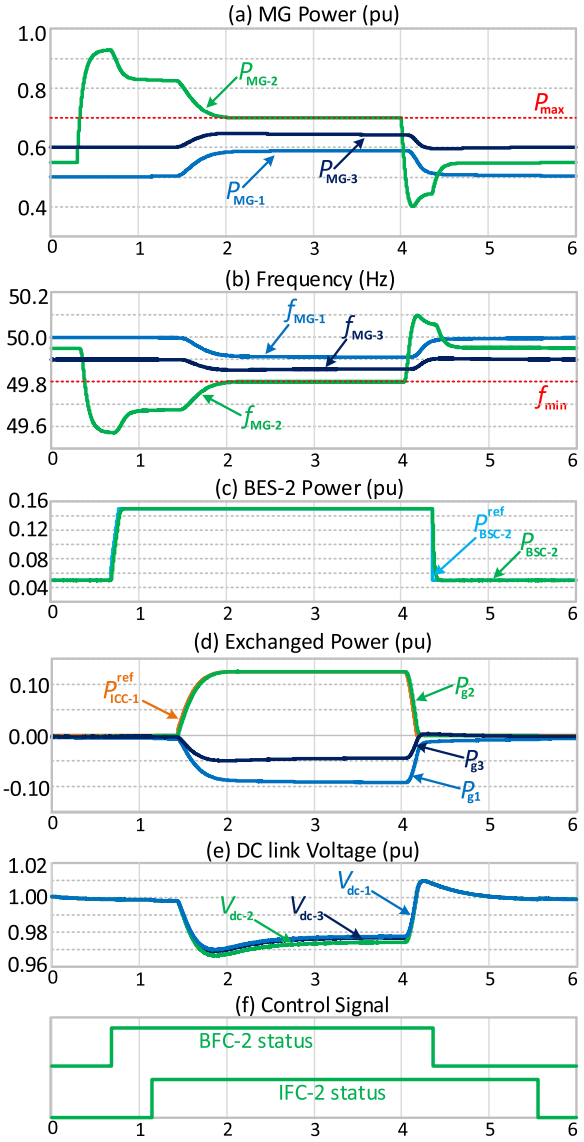

FIGURE 16. Simulation results for multiple MGs.

still below 49.8 Hz, IFC-2 will get activated at $t = 1.2$ s, and hence, the mode of operation of ICC-2 changes from the dc link voltage control to constant PQ mode. At $t = 1.5$ s, both MG-1and MG-3 start supplying power to MG-2 to alleviate the overloading situation with a power ratio of P_{g1}:$P_{g3} = 2 : 1$, as determined by their droop coefficients (see Appendix-A). It is expected that the power shared by MG-1 should be greater than MG-3 as the loading of MG-1 is less than MG-3 (See Fig. 16a). The total overload power demand for MG-2 is 0.1245 pu where the supplied power from MG-1 and MG-3 are respectively 0.091 and 0.0458 pu, as can be seen from Fig. 16d. To obtain the desired power sharing, the ratio of droop coefficients of MG-3 and MG-1 are set as $q_{MG-3} : q_{MG-1} = 2 : 1$ based on the ratio of their droop coefficients. The excess power supplied by MG-1 and MG-3, in addition to overload power of MG-2, is to overcome the line and converter losses. At $\mathbf{t} = 4$ s, the overloading of MG-2 is removed and it goes back to its normal operation, and as such, both MG-1 and MG-3 ceaseto supply power to it. The corresponding control activation signals for BFC-2 and IFC-2 are shown in Fig. 16f.

VI. CONCLUSION

A two-stage coordinated overload management technique has been proposed for systems of coupled autonomous MGs via power electronics-based converters. The proposal is based on using two self-healing agents, operating cooperatively under the predefined framework and constraints. With the proposed technique, any number of MGs can be coupled, and exchange power based on the desired (set) ratios as far as at least one MG has sufficient power to supply the power deficiency in the other MGs. The proposal has been validated under various loading conditions and SoC of BES. Through simulation studies, it has been illustrated that the proposed strategy coordinates the power exchange between the overloaded MG and its neighboring MGs as well as its local BES satisfactorily. The key benefit of the proposal is that no data communication is needed between the MGs and because of their coupling through power electronic converters, the MGs will maintain their autonomy even when exchanging power with each other.

APPENDIX- A

A. VOLTAGE TRACKING AND SWITCHING CONTROL

Voltage tracking and switching control is the most inner loop of the VSC control scheme. It is designed based on the dynamics of filter capacitor, C_f, and filter inductance, L_f at the connection point of the VSC and the MG. The dynamics can be represented in the state-space form as-

$$\dot{x} = \boldsymbol{A}\boldsymbol{x} + \boldsymbol{B_1}u_c + \boldsymbol{B_2}i_g \tag{A1}$$

where

$$\boldsymbol{A} = \begin{bmatrix} 0 & \frac{1}{C_f} \\ \frac{-1}{L_f} & \frac{-R_f}{L_f} \end{bmatrix}, \quad \boldsymbol{B_1} = \begin{bmatrix} 0 \\ \frac{V_{dc}}{2L_f} \end{bmatrix},$$

$$\boldsymbol{B_2} = \begin{bmatrix} \frac{-1}{C_f} \\ 0 \end{bmatrix} \quad \text{and } \boldsymbol{x} = \begin{bmatrix} v_c \\ i_f \end{bmatrix}$$

while u_c is the switching function and i_g is the current flowing through the coupling inductor.

It is desired that i_f only has low frequency component and all the high frequency harmonic components are filtered out or suppressed. For this purpose, a high-pass filter (with a cut-off frequency of ω_c) is introduced in the controller structure to separate the high frequency component of i_f (denoted by $\tilde{i_f}$). Hence, (A1) can be rewritten as

$$\dot{x}_c = \boldsymbol{A}_c\boldsymbol{x}_c + \boldsymbol{B}_c u_c \tag{A2}$$

where

$$\boldsymbol{A}_{\mathrm{c}} = \begin{bmatrix} 0 & \frac{1}{C_{\mathrm{f}}} & 0 \\ -\frac{1}{L_{\mathrm{f}}} & -\frac{R_{\mathrm{f}}}{L_{\mathrm{f}}} & 0 \\ -\frac{1}{L_{\mathrm{f}}} & -\frac{R_{\mathrm{f}}}{L_{\mathrm{f}}} & -\omega_c \end{bmatrix},$$

$$\boldsymbol{B}_{\mathrm{c}} = \begin{bmatrix} 0 \\ \frac{V_{\mathrm{dc}}}{2L_{\mathrm{f}}} \\ \frac{V_{\mathrm{dc}}}{2L_{\mathrm{f}}} \end{bmatrix} \quad \text{and } \boldsymbol{x}_{\mathrm{c}} = \begin{bmatrix} v_{\mathrm{c}} \\ i_{\mathrm{f}} \\ \tilde{i_f} \end{bmatrix}.$$

A suitable full state-feedback control law along with a reference input (which is the filter capacitor voltage reference, $v_{\mathrm{c}}^{\mathrm{ref}}$ in this case) can be introduced in the form of

$$u_{\mathrm{c}} = k_1\left(v_{\mathrm{c}}^{\mathrm{ref}} - v_{\mathrm{c}}\right) - k_2 i_{\mathrm{f}} - k_3\tilde{i_f} = -\boldsymbol{K}\dot{\boldsymbol{x}}_{\mathrm{c}} + k_1 v_{\mathrm{c}}^{\mathrm{ref}} \quad \text{(A3)}$$

where $\boldsymbol{K} = \begin{bmatrix} k_1 & k_2 & k_2 \end{bmatrix}$ is the state-feedback gain matrix in which k_1, k_2 and k_3 can be determined optimally by minimizing a suitable cost function using linear quadratic regulator. Through this optimization process, a robust controller can be designed with a bandwidth large enough to accurately track the low frequency sinusoidal signal (i.e., 50 Hz) with almost zero steady-state error. Therefore, (A2) can be rewritten as

$$\dot{x}_{\mathrm{c}} = \boldsymbol{A}_{\mathrm{cl}}\boldsymbol{x}_{\mathrm{c}} + \boldsymbol{B}_{\mathrm{cl}} v_{\mathrm{c}}^{\mathrm{ref}} \quad \text{(A4)}$$

where $\boldsymbol{A}_{\mathrm{cl}} = \boldsymbol{A}_{\mathrm{c}} - \boldsymbol{B}_{\mathrm{c}}\boldsymbol{K}$ and $\boldsymbol{B}_{\mathrm{cl}} = k_1\boldsymbol{B}_{\mathrm{c}}$. This controller offers infinite gain and a minimum phase margin of 60°, and hence, robustly stable. The control action can be realized through a hysteresis function with a sufficiently small band (e.g., $h = 10^{-4}$) [29], [33].

B. POWER CONTROL

Power control is the first of two outer loops employed in cascaded control structure and regulates the active and reactive power flow through the VSC. This stage of control determines the correct reference voltage across C_{f} as can be seen from Fig. 2. The conventional direct-quadrature (dq) axis power control approach can be then adopted for implanting the controller. The advantage of such type of controller is that the active and reactive power are completely decoupled and thus, can be controlled independently. Two PI controllers can be used to produce the desired d and q axis reference voltages, $v_{\mathrm{d}}^{\mathrm{ref}}$ and $v_{\mathrm{q}}^{\mathrm{ref}}$. The dynamics of coupling inductance, L_{g} and resistance, R_{g} is considered while tuning the two PI controllers using pole-zero cancellation method [40]. The d and q axis reference voltages are then converted into three-phase ac reference voltage, $v_{\mathrm{c\_abc}}^{\mathrm{ref}}$, for the filter capacitor using the measured grid angle, θ_{g}, obtained through a phase-locked loop system. The transfer function of PI controller can be given by

$$C_{\mathrm{PI}}(s) = \frac{K_{\mathrm{c}}(sT_{\mathrm{c}} + 1)}{sT_{\mathrm{c}}} \quad \text{(A5)}$$

where $T_{\mathrm{c}} = L_{\mathrm{g}}/R_{\mathrm{g}}$; and $K_{\mathrm{c}} = 2\pi f_{\mathrm{BW}}L_{\mathrm{g}}$. The parameter, f_{BW} is the closed-loop bandwidth of the controller which needs to be at least 10 times smaller than the bandwidth of the inner voltage tracking control loop. Thus, it can be assumed as a unity gain block while tuning the PI controllers of the current controller. The closed-loop transfer function of the current/power controller is then given by

$$G_{\mathrm{c}}(s) = \frac{i_{\mathrm{dq}}^{\mathrm{ref}}}{i_{\mathrm{dq}}} = \frac{1}{s\tau_{\mathrm{c}} + 1} = \frac{P_{\mathrm{ref}}}{P_{\mathrm{s}}} \quad \text{(A6)}$$

where, $\tau_c = L_{\mathrm{g}}/K_c$ is the time constant of the current controller, P_{s} is the active power output of the converter and P_{ref} is the reference power. Note that, P_{ref} is generated through any one of the four different blocks of the outermost control loop, depending on the operating mode of the converter, as shown in Fig. 2.

C. DC LINK VOLTAGE CONTROL

The dc link voltage controller is the outermost loop of the control scheme. The dynamics of the dc link capacitor voltage, V_{dc},with respect to converter output power, P_{s}, can be described as [40], [41]-

$$G_{\mathrm{dc}}(s) = \frac{V_{\mathrm{dc}}^2}{P_{\mathrm{s}}} = \left(\frac{-2}{C_{\mathrm{dc}}}\right)\frac{(s\tau_{\mathrm{dc}} + 1)}{s} \quad \text{(A7)}$$

where $\tau_{\mathrm{dc}} = 2(L_{\mathrm{f}} + L_{\mathrm{g}})P_{\mathrm{so}}/3V_{\mathrm{d}}^2$. The transfer function of $G_{\mathrm{dc}}(s)$ is a linearized small signal model where P_{so} is the steady state power output of the converter and V_{d} is the steady state d-axis voltage at the PCC of MG. DC link reference voltage can be obtained as -

$$\left(V_{\mathrm{dc}}^{\mathrm{ref}}\right)_{\mathrm{MG}-i} = V_{\mathrm{nom}} - q_{\mathrm{MG}-i}P_{\mathrm{MG}-i} \quad \text{(A8)}$$

where q and P respectively denote the dc link droop coefficient and the active power injected by the ICC and V_{nom} is the nominal voltage of the dc link (e.g., 1 pu). It is to be noted that, an active power absorption will be considered as negative. If (A8) is used to set the power desired sharing among the coupled MGs, the ratio of the power injected by MG i and j will be the reciprocal of the ratio of their droop coefficients, i.e.,

$$q_{\mathrm{MG}-i}P_{\mathrm{MG}-i} = q_{\mathrm{MG}-j}P_{\mathrm{MG}-j} \quad \text{(A9)}$$

For the purpose of designing the dc link controller that provides the minimum gain and phase margin to obtain a satisfactory performance, a generic type-2 controller can be chosen and designed to regulate the dc link voltage. The transfer function of such type of controller can be written as

$$C_{\mathrm{dc}}(s) = \frac{K_{\mathrm{dc}}(s + \omega_{\mathrm{z}})}{s(s + \omega_{\mathrm{p}})} \quad \text{(A10)}$$

The controller of $C_{\mathrm{dc}}(s)$ can be designed using the K-factor method as described in [39]. Note that, the reference power of P_{ref} in (A6) is P_{dc} in this case as can be seen from Fig. 17. The overall open-loop dc link voltage system dynamics is given by

$$G_{\mathrm{OL}}(s) = G_{\mathrm{c}}(s)G_{\mathrm{dc}}(s) = \left(\frac{-2}{C_{\mathrm{dc}}}\right)\frac{(s\tau_{\mathrm{dc}} + 1)}{s(s\tau_{\mathrm{c}} + 1)} \quad \text{(A11)}$$

TABLE 1. Technical data of the network under consideration.

Network parameters	$V_{\text{rated}} = 415\text{V}, f_{\text{nom}} = 50\text{Hz}, f_{\text{min}} = 49.8\text{Hz},$ $P_{\text{max}} = 70\text{kW}, V_{\text{dc}} = 1\text{kV}, Z_{\text{MG}} = 0.1 + j0.5\Omega$
Droop Parameters	$m = 0.01\text{Hz/kW}, n = 0.1\text{V/kVAR}$
VSC and Filters	$R_{\text{f}} = 0.1\Omega, L_{\text{f}} = 2\text{mH}, R_{\text{g}} = 0.04\Omega, L_g = 1.36\text{mH},$ $C_{\text{f}} = 25\mu\text{F}, C_{\text{dc}} = 4700\mu\text{F}$
LQR Gains	$k_1 = 58.63, k_2 = 97.18, k_3 = 1.2, \omega_c = 6283.2\text{rad/s}$
PQ Contr.	$K_{\text{c}} = 0.85, T_{\text{c}} = 0.034, \tau_{\text{c}} = 1.6\text{ms}, f_{\text{BW}} = 100\text{Hz}$
BES	$V_{\text{batt}}^{\text{ref}} = 780\text{V}, SoC_{\text{min}}^{\text{ICC}} = 55\%, SoC_{\text{nom}} = 70\%$
BFC and IFC	$K_{\text{b}} = K_{\text{ic}} = 10\text{k}, T_{\text{b}} = T_{\text{ic}} = 0.025,$ $\omega_{\text{b1}} = \omega_{\text{ic}} = 314\text{rad/s}, \omega_{\text{b2}} = 1570\text{rad/s}$
DC link controller	$K_{\text{dc}} = 222, \omega_{\text{z}} = 2.2\text{rad/s}, \omega_{\text{p}} = 1000\text{rad/s},$ $\tau_{\text{dc}} = 392.2\text{ms}, P_{\text{so}} = 100\text{kW}, V_{\text{d}} = 340\text{V}$ $V_{\text{nom}} = 1kV, q_{\text{MG}-1} = 2.5\text{V/kW}, q_{\text{MG}-3} = 5\text{V/kW}$

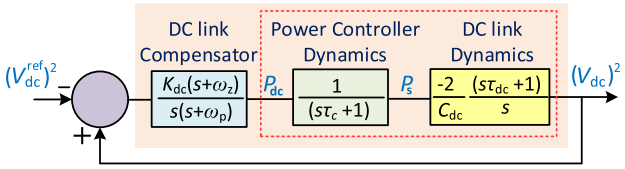

FIGURE 17. Schematic of DC link voltage control system.

Hence, $G_{\text{OL}}(s)$ is the open-loop transfer function that is needed to be considered for applying K-factor method as discussed in [42]. The design method is discussed in detail in [40]–[42] and is not repeated here.

APPENDIX-B

The technical data used in simulation for the system of coupled MGs are given in Table 1.

ACKNOWLEDGMENT

The PSIM® software license and the technical support was provided by the Murdoch University. The authors acknowledge the support and expertise received from the Renewable Energy Laboratory, Prince Sultan University, Saudi Arabia.

REFERENCES

[1] R. H. Lasseter, "MicroGrids," in *Proc. IEEE Power Eng. Soc. Winter Meeting*, vol. 1, Jan. 2002, pp. 305–308.
[2] H. Zou, S. Mao, Y. Wang, F. Zhang, X. Chen, and L. Cheng, "A survey of energy management in interconnected multi-microgrids," *IEEE Access*, vol. 7, pp. 72158–72169, 2019.
[3] Y. Yoldaş, A. Önen, S. M. Muyeen, A. V. Vasilakos, and İ. Alan, "Enhancing smart grid with microgrids: Challenges and opportunities," *Renew. Sustain. Energy Rev.*, vol. 72, pp. 205–214, May 2017.
[4] L. Ali and F. Shahnia, "Determination of an economically-suitable and sustainable standalone power system for an off-grid town in Western Australia," *Renew. Energy*, vol. 106, pp. 243–254, Jun. 2017.
[5] S. A. Arefifar and Y. A.-R.-I. Mohamed, "DG mix, reactive sources and energy storage units for optimizing microgrid reliability and supply security," *IEEE Trans. Smart Grid*, vol. 5, no. 4, pp. 1835–1844, Jul. 2014.
[6] J. G. de Matos, F. S. F. e Silva, and L. A. de S. Ribeiro, "Power control in AC isolated microgrids with renewable energy sources and energy storage systems," *IEEE Trans. Ind. Electron.*, vol. 62, no. 6, pp. 3490–3498, Jun. 2015.
[7] Z. Wang, B. Chen, J. Wang, M. M. Begovic, and C. Chen, "Coordinated energy management of networked microgrids in distribution systems," *IEEE Trans. Smart Grid*, vol. 6, no. 1, pp. 45–53, Jan. 2015.
[8] L. Sigrist, I. Egido, and L. Rouco, "Principles of a centralized UFLS scheme for small isolated power systems," *IEEE Trans. Power Syst.*, vol. 28, no. 2, pp. 1610–1617, Dec. 2013.
[9] Y.-Y. Hong, M.-C. Hsiao, Y.-R. Chang, Y.-D. Lee, and H.-C. Huang, "Multiscenario underfrequency load shedding in a microgrid consisting of intermittent renewables," *IEEE Trans. Power Del.*, vol. 28, no. 3, pp. 1610–1617, Jul. 2013.
[10] R. Paleta, A. Pina, and C. A. Santos Silva, "Polygeneration energy container: Designing and testing energy services for remote developing communities," *IEEE Trans. Sustain. Energy*, vol. 5, no. 4, pp. 1348–1355, Oct. 2014.
[11] S. A. Arefifar, Y. A.-R.-I. Mohamed, and T. H. M. EL-Fouly, "Optimum microgrid design for enhancing reliability and supply-security," *IEEE Trans. Smart Grid*, vol. 4, no. 3, pp. 1567–1575, Sep. 2013.
[12] T. Hosseinimehr, F. Shahnia, and A. Ghosh, "Power sharing control of batteries within autonomous microgrids based on their state of charge," in *Proc. Australas. Universities Power Eng. Conf. (AUPEC)*, Wollongong, NSW, Australia, Sep. 2015, pp. 1–6.
[13] W. Pei, Z. Qi, W. Deng, and Z. Shen, "Operation of battery energy storage system using extensional information model based on IEC 61850 for micro-grids," *IET Gener., Transmiss. Distrib.*, vol. 10, no. 4, pp. 849–861, Mar. 2016.
[14] M. Goyal, A. Ghosh, and F. Shahnia, "Overload prevention in an autonomous microgrid using battery storage units," in *Proc. IEEE PES Gen. Meeting|Conf. Exposit.*, Jul. 2014, pp. 1–5.
[15] M. F. Zia, E. Elbouchikhi, and M. Benbouzid, "Microgrids energy management systems: A critical review on methods, solutions, and prospects," *Appl. Energy*, vol. 222, pp. 1033–1055, Jul. 2018.
[16] H. Dagdougui, A. Ouammi, and R. Sacile, "Optimal control of a network of power microgrids using the Pontryagin's minimum principle," *IEEE Trans. Control Syst. Technol.*, vol. 22, no. 5, pp. 1942–1948, Sep. 2014.
[17] R. H. Lasseter, "Smart distribution: Coupled microgrids," *Proc. IEEE*, vol. 99, no. 6, pp. 1074–1082, Jun. 2011.
[18] L. Che, X. Zhang, M. Shahidehpour, A. Alabdulwahab, and A. Abusorrah, "Optimal interconnection planning of community microgrids with renewable energy sources," *IEEE Trans. Smart Grid*, vol. 8, no. 3, pp. 1054–1063, May 2017, doi: 10.1109/TSG.2015.2456834.
[19] F. Shahnia, S. Bourbour, and A. Ghosh, "Coupling neighboring microgrids for overload management based on dynamic multicriteria decision-making," *IEEE Trans. Smart Grid*, vol. 8, no. 2, pp. 969–983, Mar. 2017.
[20] E. Bullich-Massagué, F. Díaz-González, M. Aragüés-Peñalba, F. Girbau-Llistuella, P. Olivella-Rosell, and A. Sumper, "Microgrid clustering architectures," *Appl. Energy*, vol. 212, pp. 340–361, Feb. 2018.
[21] S. M. Ferdous, F. Shahnia, and G. Shafiullah, "Power sharing and control strategy for microgrid clusters," in *Proc. 9th Int. Conf. Power Energy Syst. (ICPES)*, Perth, WA, Australia, Dec. 2019, pp. 1–5.
[22] S. M. Ferdous, F. Shahnia, and G. Shafiullah, "Provisional energy transaction management amongst neighboring microgrids through a DC power exchange link," in *Proc. 9th Int. Conf. Power Energy Syst. (ICPES)*, Perth, WA, Australia, Dec. 2019, pp. 1–6.
[23] M. Goyal and A. Ghosh, "Microgrids interconnection to support mutually during any contingency," *Sustain. Energy, Grids Netw.*, vol. 6, pp. 100–108, Jun. 2016.
[24] S. M. Ferdous, F. Shahnia, and G. Shafiullah, "Realizing a system of coupled microgrids using a single-phase AC power exchange link," in *Proc. 9th Int. Conf. Power Energy Syst. (ICPES)*, Perth, WA, Australia, Dec. 2019, pp. 1–6.
[25] Z. Wang and J. Wang, "Self-healing resilient distribution systems based on sectionalization into microgrids," *IEEE Trans. Power Syst.*, vol. 30, no. 6, pp. 3139–3149, Nov. 2015.
[26] R. Minciardi and R. Sacile, "Optimal control in a cooperative network of smart power grids," *IEEE Syst. J.*, vol. 6, no. 1, pp. 126–133, Mar. 2012.
[27] Y. Zhang, L. Xie, and Q. Ding, "Interactive control of coupled microgrids for guaranteed system-wide small signal stability," *IEEE Trans. Smart Grid*, vol. 7, no. 2, pp. 1088–1096, Mar. 2016.
[28] I. U. Nutkani, P. C. Loh, P. Wang, T. K. Jet, and F. Blaabjerg, "Interlied AC–AC microgrids with autonomous power import and export," *Int. J. Electr. Power Energy Syst.*, vol. 65, pp. 385–393, Feb. 2015.

[29] E. Pashajavid, F. Shahnia, and A. Ghosh, "Provisional internal and external power exchange to support remote sustainable microgrids in the course of power deficiency," *IET Gener., Transmiss. Distrib.*, vol. 11, no. 1, pp. 246–260, Jan. 2017.
[30] P. C. Loh, D. Li, Y. K. Chai, and F. Blaabjerg, "Autonomous operation of hybrid microgrid with AC and DC subgrids," *IEEE Trans. Power Electron.*, vol. 28, no. 5, pp. 2214–2223, May 2013.
[31] B. John, A. Ghosh, M. Goyal, and F. Zare, "A DC power exchange highway based power flow management for interconnected microgrid clusters," *IEEE Syst. J.*, vol. 13, no. 3, pp. 3347–3357, Sep. 2019.
[32] I. U. Nutkani, P. C. Loh, and F. Blaabjerg, "Distributed operation of interlinked AC microgrids with dynamic active and reactive power tuning," *IEEE Trans. Ind. Appl.*, vol. 49, no. 5, pp. 2188–2196, Sep. 2013.
[33] F. Shahnia, A. Ghosh, S. Rajakaruna, and R. P. S. Chandrasena, "Primary control level of parallel distributed energy resources converters in system of multiple interconnected autonomous microgrids within self-healing networks," *IET Gener., Transmiss. Distrib.*, vol. 8, no. 2, pp. 203–222, Feb. 2014.
[34] M. Yazdanian and A. Mehrizi-Sani, "Distributed control techniques in microgrids," *IEEE Trans. Smart Grid*, vol. 5, no. 6, pp. 2901–2909, Nov. 2014.
[35] F. Shahnia and A. Arefi, "Eigenanalysis-based small signal stability of the system of coupled sustainable microgrids," *Int. J. Electr. Power Energy Syst.*, vol. 91, pp. 42–60, Oct. 2017.
[36] W.-Y. Chang, "The state of charge estimating methods for battery: A review," *ISRN Appl. Math.*, vol. 2013, pp. 1–7, Jul. 2013.
[37] T. Hosseinimehr, A. Ghosh, and F. Shahnia, "Cooperative control of battery energy storage systems in microgrids," *Int. J. Electr. Power Energy Syst.*, vol. 87, pp. 109–120, May 2017.
[38] S. M. Ferdous, M. Asaduzzaman Shoeb, G. Shafiullah, and M. A. Moin Oninda, "Parallel resonant converter for battery charging application," in *Proc. 9th Int. Conf. Power Energy Syst. (ICPES)*, Dec. 2019, pp. 1–6.
[39] S. M. Ferdous, M. A. M. Oninda, G. Sarowar, K. K. Islam, and M. A. Hoque, "Non-isolated single stage PFC based LED driver with THD minimization using Cúk converter," in *Proc. 9th Int. Conf. Electr. Comput. Eng. (ICECE)*, Dec. 2016, pp. 471–474.
[40] A. Yazdani and R. Iravani, *Voltage-Sourced Converters in Power Systems: Modeling, Control, and Applications*. Hoboken, NJ, USA: Wiley, 2010.
[41] A. Yazdani and R. Iravani, "An accurate model for the DC-side voltage control of the neutral point diode clamped converter," *IEEE Trans. Power Del.*, vol. 21, no. 1, pp. 185–193, Jan. 2006.
[42] S. M. Ferdous, G. M. Shafiullah, M. A. M. Oninda, M. A. Shoeb, and T. Jamal, "Close loop compensation technique for high performance MPPT using ripple correlation control," in *Proc. Australas. Univ. Power Eng. Conf. (AUPEC)*, Melbourne, VIC, Australia, Nov. 2017, pp. 1–6.

S. M. FERDOUS (Student Member, IEEE) received the bachelor's and Master of Science degrees in electrical and electronic engineering from the Islamic University of Technology (IUT), Bangladesh, in 2009 and 2012, respectively, and the Erasmus Mundus Joint master's degree in sustainable transportation and electrical power system (STEPS) coordinated by the University of Nottingham, U.K.; the University of Oviedo, Spain; the Sapienza University of Rome, Italy; and Politecnico de Coimbra, Portugal, in 2015. He is currently pursuing the Ph.D. degree with Murdoch University, Australia. He has an active teaching experience of more than six years and was working as an Assistant Professor with the Green University, Bangladesh. He has authored more than 45 refereed published book chapters, journal articles, and conference papers. His research interests include application of power electronics in microgrids, smart distribution networks, renewable power generation, and electric drives.

G. M. SHAFIULLAH (Senior Member, IEEE) received the Bachelor of Engineering degree in electrical and electronics from the Chittagong University of Engineering Technology (CUET), Bangladesh, and the Master of Engineering and Ph.D. degrees from Central Queensland University, Australia, in 2009 and 2013, respectively. He is currently a Senior Lecturer in electrical engineering with Murdoch University. He is the author of more than 120 refereed published book chapters, journal articles, and conference papers. His research interests include power systems, smart grid, renewable energy, and its enabling technologies.

FARHAD SHAHNIA (Senior Member, IEEE) received the Ph.D. degree in electrical engineering from the Queensland University of Technology, Brisbane, Australia, in 2012.

He is currently an Associate Professor with Murdoch University, Perth, Australia. He has published over 100 articles in the area of application and control of power electronic converters in distribution systems and microgrids. He currently holds the position of the IEEE Western Australia Section Chair.

RAJVIKRAM MADURAI ELAVARASAN received the B.E. degree in electrical and electronics engineering from Anna University, Chennai, and the M.E. degree in power system engineering from the Thiagarajar College of Engineering, Madurai. He has worked as an Associate Technical Operations with the IBM Global Technology Services Division. He worked as an Assistant Professor with the Department of Electrical and Electronics Engineering, Sri Venkateswara college of Engineering, Sriperumbudur, India. His research interests include renewable energy and smart grid, wind energy research, power system operation and control, and artificial intelligence control techniques. He has published papers in international journals, and international and national conferences. He was a Gold Medalist during his master's degree.

UMASHANKAR SUBRAMANIAM (Senior Member, IEEE) has over 15 years of teaching, research, and industrial research and development experience. He was an Associate Professor and the Head of VIT Vellore and a Senior Research and Development and a Senior Application Engineer in the field of power electronics, renewable energy, and electrical drives. He is currently an Associate Professor with the Renewable Energy Laboratory, College of Engineering, Prince Sultan University, Saudi Arabia. He has published more than 250 research articles in national and international journals and conferences. He has authored 12 books/chapters and 12 technical articles on power electronics applications in renewable energy, and allied areas. He received the Danfoss Innovator Award-Mentor, from 2014 to 2015 and 2017 to 2018, and the Research Award from VIT University, from 2013 to 2018. He also received the INAE Summer Research Fellowship for the year 2014. He has taken charge as the Vice Chair of the IEEE Madras Section.